CrossMark
← click for updates

# Probing bistability in Fe(II) and Co(II) complexes with an unsymmetrically substituted quinonoid ligand†‡

Margarethe van der Meer,§[a] Yvonne Rechkemmer,§[b] Frauke D. Breitgoff,[b] Sebastian Dechert,[c] Raphael Marx,[b] María Dörfel,[b] Petr Neugebauer,[b] Joris van Slageren*[b] and Biprajit Sarkar*[a]

The generation of molecular platforms, the properties of which can be influenced by a variety of external perturbations, is an important goal in the field of functional molecular materials. We present here the synthesis of a new quinonoid ligand platform containing an [O,O,O,N] donor set. The ligand is derived from a chloranilic acid core by using the [NR] (nitrogen atom with a substituent R) for [O] isoelectronic substitution. Mononuclear Fe(II) and Co(II) complexes have been synthesized with this new ligand. Results obtained from single crystal X-ray crystallography, NMR spectroscopy, (spectro)electrochemistry, SQUID magnetometry, multi-frequency EPR spectroscopy and FIR spectroscopy are used to elucidate the electronic and geometric structures of the complexes. Furthermore, we show here that the spin state of the Fe(II) complex can be influenced by temperature, pressure and light and the Co(II) complex displays redox-induced spin-state switching. Bistability is observed in the solid-state as well as in solution for the Fe(II) complex. The new ligand presented here, owing to the [NR] group present in it, will likely have more adaptability while investigating switching phenomena compared to its [O,O,O,O] analogues. Thus, such classes of ligands as well as the results obtained on the reversible changes in physical properties of the metal complexes are likely to contribute to the generation of multifunctional molecular materials.

## Introduction

The ligand 2,5-dihydroxy-1,4-benzoquinone (dhbq, Fig. 1) containing a symmetrically substituted [O,O,O,O] donor set has
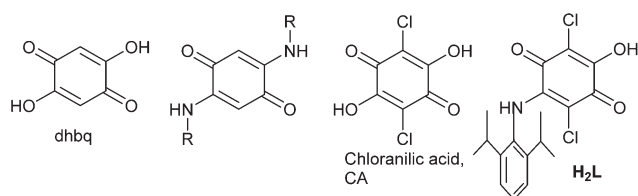


**Fig. 1** Potentially bridging quinone ligands with "O" and/or "N" donors.

[a]*Institut für Chemie und Biochemie, Freie Universität Berlin, Fabeckstraße 34-36, D-14195 Berlin, Germany. E-mail: biprajit.sarkar@fu-berlin.de*
[b]*Institut für Physikalische Chemie, Universität Stuttgart, Pfaffenwaldring 55, D-70569 Stuttgart, Germany. E-mail: ipcjosl@ipc.uni-stuttgart.de*
[c]*Institut für Anorganische Chemie, Georg-August-Universität Göttingen, Tammannstraße 4, D-37077 Göttingen, Germany*

been extensively used in coordination chemistry.[1] In recent years, the combination of dhbq with Co(II) showed valence tautomerism (VT).[2] A related ligand, chloranilic acid (CA, Fig. 1) and its derivatives, were also used with Fe(II),[3] to generate spin crossover (SCO) properties[4] and with Co(II),[5] to generate VT. In the Co(II) complexes with dhbq, switching of the spin state was achieved both as a function of temperature and pressure.[2] The redox-active nature of the metal centers and the ligands make such systems ideal for investigating redox-induced spin state switching. However, such a process has hardly been investigated for these metal complexes.[1–3,5] In both dhbq and CA the ligands contain an all [O] donor set, thus limiting chemical modification of such ligands only to direct substitution on the central ring. We[6,7] and others[8] have used the [NR] (nitrogen atom with a substituent R) for [O] isoelectronic analogy to modify dhbq and related ligands to generate ligands with symmetrical [O,N,O,N] donor sets (Fig. 1). The "R" handle in the [NR] group provides ample opportunities for steric, electronic and solubility tuning of the metal complexes, a fact that is not possible with dhbq or CA. Thus, functional metal complexes with such [O,N,O,N] donor sets have been useful for investigating electron transfer processes, spin state switching, spin–spin coupling and other properties.[6] In these ligands with an [O,N,O,N] donor set, the central six-membered ring is always symmetrically substituted with the heteroatom donors.

Examples of potentially bridging quinonoid ligands with unsymmetrically substituted donor groups such as [O,O,O,N] and their metal complexes are rare.[6a]

In our pursuit of generating new quinonoid ligand platforms with one or more [NR] donors, we have now turned our attention to modifying the CA ligand. To the best of our knowledge, CA has never been modified through the [NR] for [O] substitution to generate unsymmetrically substituted ligands with an [O,O,O,N] donor set, even though there has been a recent example of modified CA with a symmetrically substituted [O,N,O,N] donor set[3d] (Fig. 1). Access to ligands with such unsymmetrical substitution is likely to make studies of preferential coordination of metal centers at one or the other binding site ([O,O] vs. [O,N]) possible. The aforementioned complexes could then be used for generating heterobimetallic complexes, for addressing the targeted switching of a particular metal center in homobimetallic complexes, or for implementing two-qubit gates. In the last of these, the two metal centers that act as the two qubits have to be distinct.[9] These goals are important in the field of functional molecular materials but are difficult to achieve with symmetrically substituted quinonoid ligands containing a [O,O,O,O] or [O,N,O,N] donor set.

In the following, we present the synthesis of the unsymmetrically substituted ligand 2-[(2',6'-diisopropyl)anilino)]-3,6-dichloro-5-hydroxy-1,4-benzoquinone (H$_2$L, Fig. 1), its Fe(II) complex [(tmpa)Fe(HL)](BF$_4$), [1]BF$_4$ and its Co(II) complex [(tmpa)Co(HL)](BF$_4$), [2]BF$_4$ (tmpa = tris(2-methylpyridyl) amine). Results from X-ray crystallography, $^1$H NMR spectroscopy, electrochemistry, multi-frequency EPR spectroscopy, FIR spectroscopy, UV-vis-NIR spectroelectrochemistry, and SQUID magnetometry are discussed below to show the changes in the spin state in these systems as a function of multiple external perturbations and to describe their electronic structures.

# Results and discussion

## Synthesis and crystal structures

The reaction of CA with 2,6-diisopropylaniline in acetic acid under reflux, followed by recrystallization led to the formation of H$_2$L (Scheme 1 and Experimental section).

We had reported earlier on a similar method to prepare ligands with an [O,N,O,N] donor set (Fig. 1) starting from dhbq.[6a] In those ligands, usually two of the [O] in dhbq are substituted with two [NR] groups leading to the formation of a symmetrically substituted quinonoid ligand as the major product. In the present case the only product that we could isolate was the one where only one of the [O] in CA was substituted with a [NR] group leading to the unsymmetrically substituted ligand H$_2$L that has an [O,O,O,N] donor set. The electron-poor nature of the CA ring because of the presence of the chloro substituents is likely responsible for the sluggishness of CA to undergo such a substitution reaction. The net result however is the formation of an unsymmetrically substituted H$_2$L ligand, examples of which are rare in the literature.[6a,h] The purity and structure of H$_2$L was established using a combination of $^1$H and $^{13}$C NMR data and elemental analyses (see Experimental section).

The complexes were synthesized in a one-pot reaction using Fe(BF$_4$)$_2$·6H$_2$O or Co(BF$_4$)$_2$·6H$_2$O, tmpa, H$_2$L and NEt$_3$ (Scheme 1 and Experimental section). Recrystallization from CH$_2$Cl$_2$/n-hexane led to the formation of pure, crystalline materials. The initial purity of the complexes was checked through elemental analyses that showed an excellent match between the calculated and experimental values of C, H and N. The final confirmation of the structure came from single crystal X-ray diffraction studies. All further studies on these complexes were performed with the pure crystalline material.

Single crystals of [1]BF$_4$ and [2]BF$_4$ (Fig. 2) were obtained as CH$_2$Cl$_2$ solvates. For both complexes bond length analysis
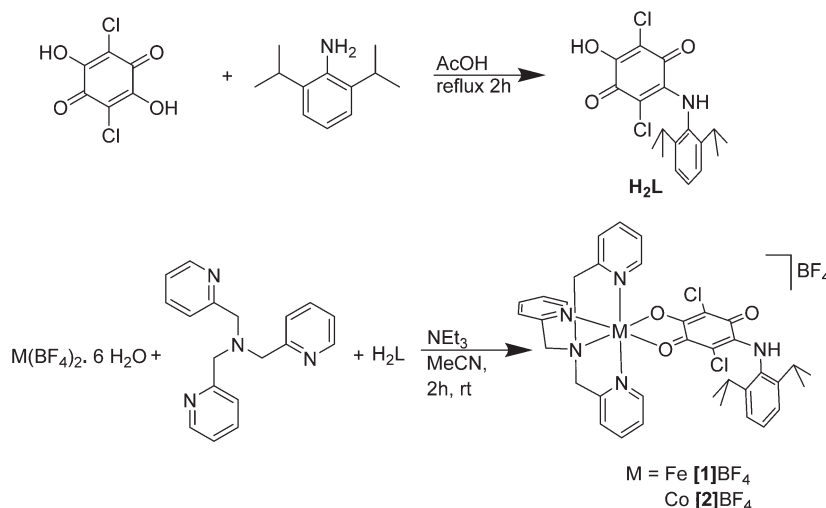


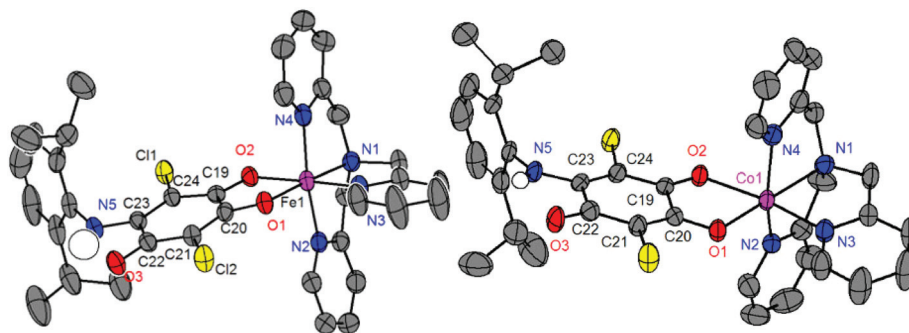**Scheme 1** Synthesis of the ligand (top) and of the metal complexes (bottom).

**Fig. 2** Perspective view of [**1**]BF$_4$·2CH$_2$Cl$_2$ (left) and [**2**]BF$_4$·2CH$_2$Cl$_2$ (right). The ellipsoids are drawn at 50% probability. Hydrogen atoms (except N–H), solvent molecules and counter-ions are omitted for clarity.

**Table 1** Selected bond lengths (Å) and bond angles (°) of [**1**]BF$_4$·2CH$_2$Cl$_2$ and [**2**]BF$_4$·2CH$_2$Cl$_2$

|  | [**1**]BF$_4$·2CH$_2$Cl$_2$ | [**2**]BF$_4$·2CH$_2$Cl$_2$ |  | [**1**]BF$_4$·2CH$_2$Cl$_2$ | [**2**]BF$_4$·2CH$_2$Cl$_2$ |
|---|---|---|---|---|---|
| M–N1[a] | 1.984(3) | 2.193(4) | C21–C22 | 1.418(5) | 1.413(6) |
| M–N2 | 1.973(4) | 2.107(4) | C22–C23 | 1.521(6) | 1.546(6) |
| M–N3 | 1.927(3) | 2.065(4) | C23–C24 | 1.392(5) | 1.380(6) |
| M–N4 | 1.957(4) | 2.090(4) | C24–C19 | 1.411(5) | 1.415(5) |
| M–O1 | 1.936(3) | 2.034(3) | C20–O1 | 1.285(5) | 1.275(5) |
| M–O2 | 1.978(3) | 2.158(3) | C19–O2 | 1.263(5) | 1.240(5) |
| C19–C20 | 1.490(5) | 1.524(6) | C22–O3 | 1.241(5) | 1.233(5) |
| C20–C21 | 1.368(6) | 1.369(6) | C23–N5 | 1.342(5) | 1.327(5) |
| N1–M–O1[a] | 176.5(1) | 172.6(1) | N2–M–N3 | 89.2(2) | 94.4(2) |
| N2–M–N4 | 167.0(2) | 153.7(2) | N2–M–O1 | 93.3(1) | 96.7(1) |
| N3–M–O2 | 175.4(1) | 171.7(1) | N2–M–O2 | 91.1(1) | 107.4(1) |
| N1–M–N2 | 83.5(1) | 78.2(1) | N3–M–N4 | 91.6(2) | 94.6(2) |
| N1–M–N3 | 85.3(1) | 80.8(1) | N3–M–O1 | 93.5(1) | 94.1(1) |
| N1–M–N4 | 83.7(1) | 78.9(1) | N4–M–O1 | 99.7(1) | 107.2(1) |
| O1–M–O2 | 81.8(1) | 77.5(1) | N4–M–O2 | 89.1(1) | 85.9(1) |

[a] M = Fe for [**1**]BF$_4$·2CH$_2$Cl$_2$ and M = Co for [**2**]BF$_4$·2CH$_2$Cl$_2$.

within the (**HL**$^-$) ligand showed bond localization within the quinone ligand.[6,8k] This is apparent for example from the bond lengths of 1.367(6) and 1.416(6) Å for the C20–C21 and C21–C22 bonds respectively in [**1**]BF$_4$ (Table 1). Accordingly, the C20–O1 bond is slightly longer than C22–O3. A similar situation is also observed in the "upper half" of the ligand (**HL**$^-$). The C22–C23 and C19–C20 bond lengths are around 1.5 Å and in the region of a C–C single bond. The donor atoms are thus best described as being a phenoxide type "O$^-$" and a neutral ketotype "O" donor. One proton is accordingly localized on the N-atom, with the ligand retaining its substituted *p*-quinone type form. The metal coordination takes place preferentially through the [O,O] donor site which is easier to deprotonate in the H$_2$L ligand. This difference in basicity and less steric crowding at the [O,O] donor site is also the reason for the exclusive formation of mononuclear complexes in the present case. A similar bonding situation is observed within the (**HL**$^-$) ligand in the Co(II) complex [**2**]BF$_4$ (Table 1).

The Fe–O and Fe–N bond distances in [**1**]BF$_4$ are all shorter than 2 Å (Table 1). These values indicate the existence of a low spin (LS) state (LS-t$_{2g}^6$ configuration in a simplified model for an octahedral complex) for the Fe(II) center at the measured temperature of 133 K.[4] Accordingly, the octahedron around the

Fe(II) center is a compact one as can be seen from only a small deviation of the angles from the ideal 90° (Table 1). In contrast, the Co–O and Co–N distances in [**2**]BF$_4$ are all longer than 2 Å, and the octahedron around the Co(II) centers displays large distortions as can be seen from the large deviations of bond angles around it from the ideal 90° (Table 1). These data are an indication of a distorted, six-fold coordinated high spin (HS) Co(II) center (HS-t$_{2g}^5$e$_g^{*2}$ configuration in a simplified model for an octahedral complex).[6d]

### Electrochemistry and UV-vis-NIR spectroelectrochemistry

The electron transfer properties of the two complexes were investigated by a combination of electrochemistry and UV-vis-NIR spectroelectrochemistry. Both complexes display a quasi-reversible one electron reduction, the potential of which is close to −1 V *vs.* Fc/Fc$^+$ (Fig. 3). UV-vis-NIR spectroelectrochemical measurements did not lead to the regeneration of the starting spectrum on scanning the potential back, precluding the spectroscopic characterization of the one-electron reduced form. However, the appearance of the reduction step at similar potentials for both complexes, together with earlier reports on similar compounds,[6d] makes an assignment of the reduction step on the (**HL**$^-$) ligand reasonable.
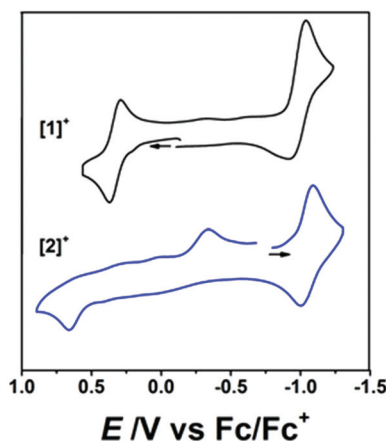
**Fig. 3** Cyclic voltammogram of [1]$^+$ (in CH$_2$Cl$_2$/0.1 M Bu$_4$NPF$_6$) and [2]$^+$ (in CH$_3$CN/0.1 M/Bu$_4$NPF$_6$) measured at 295 K.

In contrast to the reduction step, the oxidation of both compounds appears at different potentials, and has very different features. For [1]$^+$, an electrochemically and chemically reversible oxidation step with a half-wave potential of 0.32 V is observed. All features of this peak, together with results from UV-vis-NIR spectroelectrochemistry experiments (see below) show a chemically as well as an electrochemically reversible electron transfer step, leading likely to the generation of a HS Fe$^{III}$ center at the measured temperatures in fluid solution.[3d] For [2]$^+$, the forward wave is observed at 0.66 V (Fig. 3) and the re-reduction wave appears at −0.30 V. In UV-vis-NIR spectroelectrochemical experiments, the starting spectrum of [2]$^+$ is re-generated on scanning the potential back to −0.30 V after the oxidation step (see below). These results are an indication of an electron transfer-chemical (EC) reaction or more complicated mechanism accompanied by spin state changes. Starting from a HS Co$^{II}$ center in [2]$^+$, that is a distorted octahedral d$^7$ center, oxidation is expected to lead to a LS Co$^{III}$ species (see NMR discussion below). Such a low-spin d$^6$ system (LS-t$_{2g}^6$ configuration in a simplified model) will certainly contain shorter Co–ligand bond lengths and display smaller distortions from a perfect octahedral geometry as compared to the HS-Co$^{II}$ form. The aforementioned process is usually associated with large reorganization energy. Additionally, there is a possibility of the formation of different isomers during the oxidation process (see discussion below). All these phenomena contribute to the EC mechanism. The HS Co$^{II}$ form is however regenerated on re-reducing the complex, making the process chemically reversible.

In the UV-vis-NIR spectrum, [1]$^+$ displays a weak long wavelength band at 845 nm and a weak shoulder at 620 nm (Fig. 4). For [2]$^+$ the weak long wavelength band appears at 561 nm. Quinonoid ligands such as H$_2$L usually display weak π to π* transitions in the visible region.[6a] For the present complexes we tentatively assign these bands to a mixture of such quinone ligand centered transitions and metal to ligand charge transfer (MLCT) transitions from filled d orbitals based on the metal to
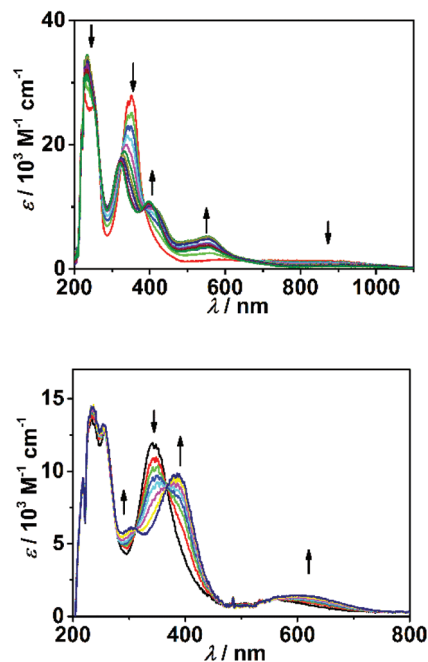


**Fig. 4** Changes in the UV-vis-NIR spectrum of [1]$^+$ in CH$_2$Cl$_2$/0.1 M Bu$_4$NPF$_6$ (top) and of [2]$^+$ in CH$_3$CN/0.1 M Bu$_4$NPF$_6$ (bottom) during oxidation.

low lying empty orbitals on the quinone ligand. The bands at 351 nm for [1]$^+$ and 342 nm for [2]$^+$ are likely MLCT bands where the target orbitals are higher-lying empty orbitals based on the ligands. Further bands at higher energies are all ligand based transitions (Table 2).

On one electron oxidation, the long wavelength bands for both complexes lose intensity and new bands appear at 554 nm for [1]$^{2+}$ and at 613 nm for [2]$^{2+}$ (Fig. 4). Furthermore, both the bands at 351 nm ([1]$^+$) and 342 nm ([2]$^+$) for the starting complexes lose intensity on one electron oxidation. This fact is in accordance with the assignment of these bands as MLCT bands (metal centered oxidation, see below). New bands appear at 398 nm for [1]$^{2+}$ and at 388 nm for [2]$^{2+}$, which are assigned to ligand to metal charge transfer (LMCT) transitions from filled orbitals on the quinone ligand to empty d orbitals on the oxidized metal centers. As expected, the oxidation steps do not have much influence on the bands that appear at further higher energies (Fig. 4). For both complexes, scanning

**Table 2** UV-vis-NIR data of the complexes in various redox forms[a]

|  | $\lambda$/nm ($\varepsilon$/10$^3$ M$^{-1}$ cm$^{-1}$) |
| --- | --- |
| [1]$^+$ | 255 (27.1); 351 (28.1); 620 sh, 845 (1.37) |
| [1]$^{2+}$ | 232 (31.4); 320 (17.1); 398 (11.0); 554 (3.68) |
| [2]$^+$ | 231 (13.6); 257 (12.6); 342 (11.7); 561 (1.25) |
| [2]$^{2+}$ | 235 (14.4); 255 (13.3); 305 (6.13); 388 (9.87); 613 (1.50) |

[a] From OTTLE spectroelectrochemistry in CH$_2$Cl$_2$ for [1]$^+$ and CH$_3$CN for [2]$^+$, 0.1 M Bu$_4$NPF$_6$.

the potential back, led to the quantitative regeneration of the spectra corresponding to the starting species, thus indicating the reversible nature of the oxidation steps.

## Investigation of spin state changes through multiple external perturbations

Temperature- and field-dependent magnetic susceptibility measurements of [**1**]BF$_4$ (Fig. 5 and S1‡) show a sudden decrease in the $\chi T$ product from a value of 1.96 cm$^3$ K mol$^{-1}$ at room temperature to a value of 0.52 cm$^3$ K mol$^{-1}$ at 140 K. This behaviour is indicative of spin crossover from a high spin state (HS, $S = 2$) at high temperatures to a low spin state (LS, $S = 0$) at low temperature, with a concurrent decrease of the magnetic moment. On further lowering of the temperature, $\chi T$ remains constant until it rapidly drops below 8 K which we attributed to zero-field splitting. $\chi T$ does not reach the expected value of an $S = 2$ ion in the HS state (3.0 cm$^3$ K mol$^{-1}$ for $g = 2$), nor is the $\chi T$ product zero at low temperatures. These observations indicate an incomplete SCO in the solid state. Such incomplete SCO processes have been observed previously.[3d,4d,e] To simulate the susceptibility data, an Ising-like model was applied,[10] with the best fit shown in Fig. 5. The simulation revealed a transition temperature of $T_{1/2} = 251 \pm 1$ K. The cooperativity parameter, which is a measure of the influence of cooperative intermolecular interactions on the SCO process was determined to be $J = 167 \pm 2$ cm$^{-1}$. Furthermore, the energy gap between HS and LS states was found to be $\Delta = 226 \pm 15$ cm$^{-1}$. The HS molar fraction is 60% at 300 K and 16% at low temperature (Fig. 5).

Photomagnetic experiments were carried out to study whether the conversion from LS to HS in [**1**]BF$_4$ can also be induced by irradiation, known as light induced excited spin state trapping (LIESST).[11] Upon excitation with green laser light (532 nm) the magnetic susceptibility increases (Fig. 5). The higher $\chi T$ value corresponds to a higher fraction of the sample being present in the HS state, hence the conversion from the LS to HS state was induced by irradiation. The relative change in magnetic moment on irradiation is rather weak.
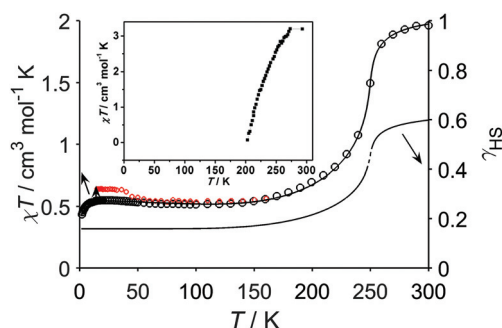
This is typically due to the high-spin form also absorbing light at the irradiation wavelength. This has two consequences: (i) the light does not penetrate very far into the sample, (ii) reverse SCO can occur, leading to a steady state distribution of high- and low-spin species. After switching off the laser and measuring the magnetic susceptibility while slowly warming the sample to 300 K the $\chi T$ product first remains stable and then decreases until it coincides with the data without irradiation. This indicates that [**1**]BF$_4$ undergoes thermal relaxation at 42 K. This characteristic temperature is called $T_{\text{LIESST}}$ or critical temperature in the literature. The occurrence of LIESST was further confirmed by an isothermal relaxation measurement at 15 K, where the influence of sample heating immediately after commencing the irradiation can be clearly seen (Fig. S2‡). Upon discontinuation of the irradiation, the magnetic moment rapidly increases due to sample cooling, followed by a slow decay due to thermal relaxation.

The complex [**1**]$^+$ also displays SCO behaviour in a CD$_2$Cl$_2$ solution (Fig. 5, inset). At 303 K, a $^1$H NMR spectrum is obtained which spans the region between 0 and 75 ppm, confirming the paramagnetic nature of the Fe$^{II}$ center (Fig. S3‡). On cooling to 183 K all signals are observed within the 0 to 10 ppm range confirming the conversion of [**1**]$^+$ to the diamagnetic, LS Fe$^{II}$ form. A $T_{1/2}$ of 240 K was determined for the SCO process in solution.

To study the electronic structure of [**1**]BF$_4$, EPR spectra were recorded at X-band frequency (Fig. S4‡), where a clear resonance line attributed to the HS species is observed. In the high-frequency EPR (HFEPR), no corresponding signal was observed. This could be due to HS to LS conversion as a result of the 1.5 tons of pressure used in preparing the HFEPR pellet. An enhancement of the LS species under pressure has been previously found.[12] We have used the standard Hamiltonian for Zeeman splitting and second rank axial ($D$) and rhombic ($E$) zero-field splitting to simulate the data: $\mathscr{H} = g\mu_B B + D(\hat{S}_{z^2} - S(S + 1)/3) + E(\hat{S}_{x^2} - \hat{S}_{y^2})$. Combining the results of magnetometric and spectroscopic measurements the best simulations were obtained with $g = 2.16 \pm 0.05$, $D = 2 \pm 0.5$ cm$^{-1}$ and $E = 0.047 \pm 0.0002$ cm$^{-1}$ (Fig. S4‡). These values are not untypical for HS iron(II).

In the case of [**2**]BF$_4$, we have used far-infrared (FIR) spectroscopy to determine the zero-field splitting (ZFS). The spectra (Fig. 6) show a clear feature at 66 cm$^{-1}$. Due to the strong distortion of the octahedral coordination of Co$^{II}$ we can assume the orbital angular momentum to be quenched, resulting in spin-only magnetism with $S = 3/2$.[6d] The excitation energy corresponds to $2|D|$ and therefore, $|D| = 33 \pm 2$ cm$^{-1}$. EPR spectra of [**2**]BF$_4$ were recorded at 9.5 and 300 GHz (Fig. 7). At the X band frequency signals at 150 and 340 mT were observed. The resonance lines in the HFEPR (300 GHz) spectrum are located at 3.8, 4.1, 4.9 and 5.4 T and at 10.3 and 10.7 T. Preliminary fits showed that the EPR spectra can only be simulated by assuming two different species A and B, each showing a different set of anisotropic $g$ values, but the same $D$ value. The spectra were modelled with a positive zero-field



**Fig. 5** Temperature dependence of $\chi T$ for [**1**]BF$_4$ measured at 1000 Oe (black symbols), photo-induced change in magnetization (red symbols) by irradiation with green laser light ($\lambda$ = 532 nm). The solid line is the fit (see text), and the dashed line is the high-spin fraction (right hand scale). The inset shows the temperature dependence of $\chi T$ obtained from solution $^1$H NMR data.
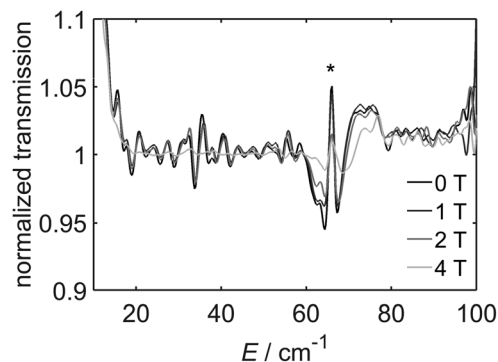
**Fig. 6** FIR spectra of **[2]**BF$_4$ recorded at 9 K and 0–4 T. The spectra have been normalized by dividing by the spectrum recorded at 6 T. A measurement artefact is marked with *. The transition at 65 cm$^{-1}$ which changes intensity with the magnetic field corresponds to $2D$ in the absence of rhombic zero-field splitting.
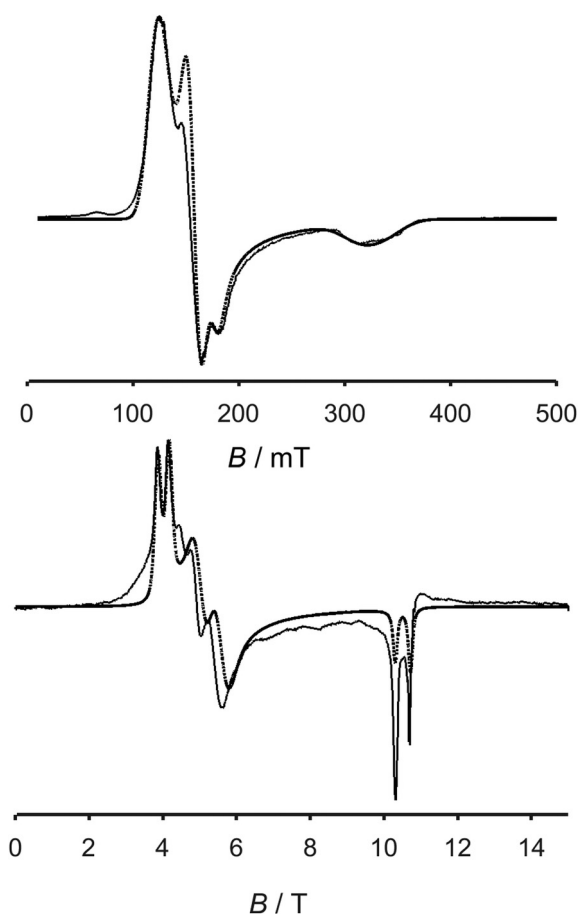


**Fig. 7** X-band EPR (top) and HFEPR (300 GHz, bottom) spectra recorded on pressed powder samples of **[2]**BF$_4$. The light grey lines are the fits using parameters given in the text.

splitting parameter $D$ of +33(2) cm$^{-1}$, $g$ values of 2.78(5), 2.14(2) and 2.08(3) for species A and $g$-values of 2.58(3), 1.93(4) and 2.00(2) for species B. HFEPR is very sensitive to small differences in the structure that might not be observable in

magnetic or crystallographic measurements. Also, the low temperature structure of **[2]**BF$_4$ is not known, but might feature two slightly different molecules in the unit cell. A hyperfine coupling of $A_{\parallel} = 180$ MHz was included in order to better reproduce the X-band signal at higher fields (Fig. 7). Two crystallographic positions for Co$^{II}$ semiquinonate complexes have been observed by others as well.[13]

Magnetic susceptibility measurements were carried out to study whether the complex **[2]**BF$_4$ displays valence tautomerism (VT). The $\chi T$ product decreases gradually with $T$ from 300 to 50 K. Below 50 K the decline is steeper due to zero-field splitting until a value of 1.44 cm$^3$ mol$^{-1}$ K is reached at 1.8 K (Fig. S5‡). As the decline of $\chi T$ with $T$ is gradual we conclude that complex **[2]**BF$_4$ does not show VT to any substantial extent in the temperature range studied here. $\chi T$ was simulated, assuming high spin cobalt(II), with $D = +33$ cm$^{-1}$, $g_1 = 1.58$, $g_2 = 1.93$, and $g_3 = 2.00$, the gradual decline of $\chi T$ being modelled as temperature independent paramagnetism ($\chi_{TIP} = 900 \times 10^{-6}$ cm$^3$ mol$^{-1}$) (Fig. S5‡). The experimental values are in good agreement with the simulated values supporting the assumption of spin-only magnetism and correspond well with the reported values for HS Co$^{II}$.[14] The magnetization curve measured at 1.8 K shows a saturation value of 2.06$\mu_B$ (inset in Fig. S5‡), and was also modelled successfully with the same parameters. The complex **[2]**$^+$ was chemically oxidized with NOBF$_4$. The resulting **[2]**$^{2+}$ form was found to be diamagnetic and delivers a $^1$H NMR spectrum that fits with a LS Co$^{III}$ form (Fig. 8). This result thus confirms a metal-centered oxidation as discussed in the spectroelectrochemistry section above. Whereas the freshly dissolved solid delivered a spectrum corresponding to only one isomer, on leaving the solution for several hours, the formation of a second positional isomer in solution was observed (Fig. 8 and S6‡). These results thus confirm the discussion on reorganization after the oxidation step as stated in the electrochemistry section above. The spin state of the **[2]**$^+$ species can thus be switched from $S = 3/2$ for a HS-Co$^{II}$ center to $S = 0$ for a LS-Co$^{III}$ center by a simple reversible one-electron step.[6d] The potentially bridging ligand, **HL**$^-$, the types of which are known to take part in electron transfer, does not participate in the oxidation process of **[2]**$^+$. The quintessentially non-innocent quinone ligand thus acts as innocent for the present case, thus displaying the need for specifying a particular metal–ligand combination when discussing ligand non-innocence.[15]

## Conclusions

Summarizing, we have presented here the synthesis of a rare unsymmetrically substituted, potentially bridging quinone ligand. A mononuclear Fe$^{II}$ and a Co$^{II}$ complex with this ligand has been synthesized and structurally characterized. The Fe$^{II}$ complex displays SCO in the solid state and in solution with a transition temperature of 251 K in the solid state. The spin state of this complex can be switched either by varying the temperature or pressure. The same complex also shows a
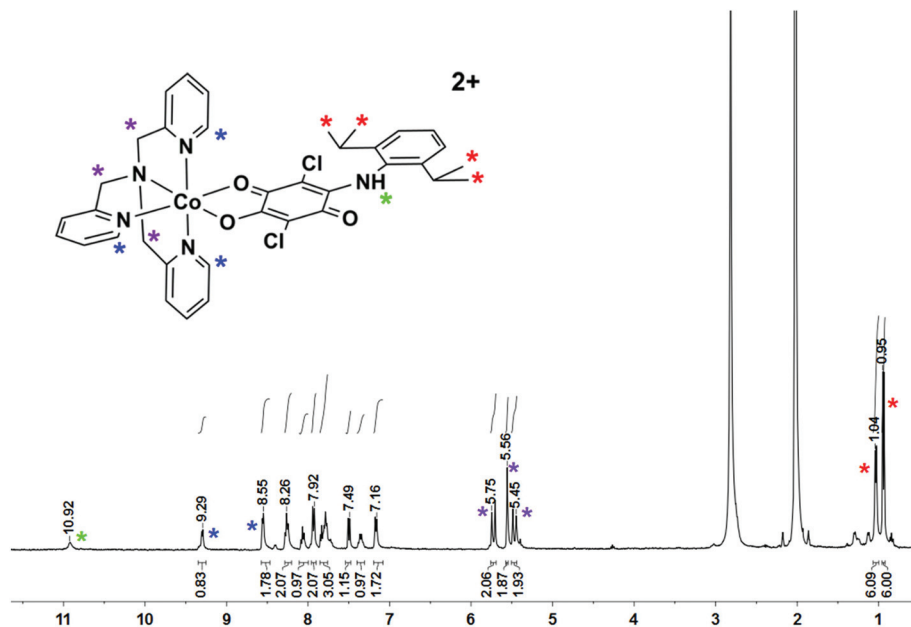
**Fig. 8** $^1$H-NMR of [2]$^{2+}$ directly measured after dissolving the sample.

LIESST effect with a thermal relaxation at 42 K. The Co$^{II}$ complex displays a redox-induced spin state switching, delivering a LS Co$^{III}$ complex on performing a reversible one electron transfer step. The potentially non-innocent (**HL**$^-$) ligand thus remains innocent on the oxidative side. FIR spectroscopy delivers a $D$ value of +33 cm$^{-1}$ for [2]BF$_4$. We have used a combination of crystallographic, (spectro)electrochemical, spectroscopic and magnetic methods to probe the electronic structures and the changes in magnetic properties of the molecules in various states. In particular, the combination of FIR spectroscopy, magnetism and (HF)EPR spectroscopy has allowed us to determine the spin Hamiltonian parameters of the complexes accurately. The results presented here show the potential of these newly synthesized quinone ligands for generating complexes displaying bistability as a function of multiple external perturbations. Future work will target complexes with higher nuclearity with an aim of incorporating multiple switching units within the same molecule.

## Experimental section

### General considerations

Tris(2-methylpyridyl)amine (tmpa) was prepared according to a literature known procedure.[16] All other reagents were commercially available and were used as received. All solvents were dried and distilled using common techniques unless otherwise mentioned. All reactions are carried out under a N$_2$-atmosphere.

### Instrumentation

Cyclic voltammetry was carried out in 0.1 M Bu$_4$NPF$_6$ solution using a three-electrode configuration (Pt or glassy carbon working electrode, Pt counter electrode, Ag wire as pseudo-reference) and PAR Versa STAT 4 potentiostat. The ferrocene/ferrocenium (Fc/Fc$^+$) couple served as an internal reference. UV-vis-NIR absorption spectra were recorded on an Avantes spectrometer system: Ava Light-DH-BAL (light source), AvaSpec-ULS2048 (UV-vis-detector) and AvaSpec-NIR256-2.5TEC (NIR-detector). Spectroelectrochemical measurements were carried out using an optically transparent thin layer electrochemical (OTTLE) cell.[17] Elemental analysis was performed on a Perkin Elmer Analyser 240. Mass spectrometry experiments were carried out on a Bruker Daltonics Mictrotof-Q mass spectrometer and mass spectrum simulations were done with mmass.

### X-ray crystallography

Crystal data and details of the data collections are given in Table S1.‡ X-ray data were collected on a STOE IPDS II diffractometer and BRUKER AXS (graphite monochromated Mo-Kα radiation, $\lambda$ = 0.71073 Å) by the use of $\omega$ scans. The structures were solved by direct methods (SHELXS-97) and refined on $F^2$ using all reflections with SHELXL-2014.[18a] Non-hydrogen atoms were refined anisotropically. Most hydrogen atoms were placed in calculated positions and assigned to an isotropic displacement parameter of $1.2/1.5U_{eq}(C)$. The nitrogen-bound hydrogen atoms were refined freely. Both compounds contain disordered CH$_2$Cl$_2$ solvent molecules. In the case of [1]BF$_4$·2CH$_2$Cl$_2$ two CH$_2$Cl$_2$ are disordered about inversion centers. One was refined at 1/2 occupancy, the other one shows an additional positional disorder and each part was refined at 1/4 occupancy. The occupancy factors of the third solvent molecules were refined to 0.880(6)/0.120(6). DFIX restraints ($d_{C-Cl}$ = 1.79 Å, $d_{Cl\cdots Cl}$ = 2.8 Å) and EADP constraints

were applied to model the disorder. In the case of [2]$BF_4 \cdot 2CH_2Cl_2$ two $CH_2Cl_2$ are disordered about inversion centers. Both were refined at 1/2 occupancy. The occupancy factors of the third solvent molecules were refined to 0.777(6)/0.223(6). DFIX restraints ($d_{C-Cl}$ = 1.79 Å) and EADP constraints were used to model the disorder. Furthermore the $BF_4^-$ anion of [1]$BF_4 \cdot 2CH_2Cl_2$ is disordered (occupancy factors: 0.637(6)/0.363(6)). EADP constraints were used for anisotropic refinement of the counter ion.

Face-indexed absorption corrections for [1]$BF_4 \cdot 2CH_2Cl_2$ were performed numerically with the program X-RED.[18b] SADABS,[18c] CCDC 971157 ([1]$BF_4$) and 1052194 ([2]$BF_4$) contain the cif files for this work.

### Magnetic susceptibility measurements

The magnetic measurements on powder samples were performed with a MPMS 3 SQUID magnetometer for [2]$BF_4$ and with a MPMS-XL7 SQUID magnetometer for [1]$BF_4$, both from Quantum Design. Samples were slightly pressed, Teflon wrapped powder pellets. For the temperature-dependent measurements below 50 K an external magnetic field of 1000 Oe was applied; for measurements above 40 K 10 000 Oe was applied. The molar susceptibility data were corrected for diamagnetic contributions by subtracting $\chi_m^{dia} = -0.5 \times MM \times 10^{-6}$ $cm^3$ $mol^{-1}$. The molar susceptibility data of [1]$BF_4$ have been corrected for diamagnetic impurities as well. Magnetic susceptibility measurements in solution were analyzed using the Evans method.[19]

For the photomagnetic experiments an external magnetic field of 1000 Oe was applied, [1]$BF_4$ was cooled down to 1.8 K and then heated to 15 K. Irradiation of the sample was performed by coupling a 532 nm laser beam through an optical fiber to the cavity of the MPMS-XL7 SQUID magnetometer. The sample was irradiated until no further increase in susceptibility was observed. After switching off the laser the magnetic susceptibility was measured while warming the sample to 300 K at a rate of 1 K $min^{-1}$ (inset in Fig. 5). The photomagnetic experiments were carried out on a thin layer of sample in vacuum grease and scaled to match the data measured for a heavier and thus more accurately weighed sample of [1]$BF_4$.

### EPR spectroscopy

X-band EPR spectra at 9.47 GHz were recorded using a Bruker EMX spectrometer equipped with a continuous flow cryostat. HFEPR spectra were measured with a home-built spectrometer at frequencies between 95 and 380 GHz. For the HFEPR measurements the samples were pressed into pure pellets to prevent orientation in the magnetic field. Simulations were performed with Easyspin.[20]

### FIR spectroscopy

Far infrared (FIR) spectra were recorded on a Bruker 113v FTIR spectrometer equipped with a mercury vapour light source and an Infrared Laboratories pumped Si bolometer. The samples were studied as pure pellets attached to a sample holder inserted into an 8T Oxford Instruments Spectromag 4000 optical cryomagnet. The sample holder permitted in situ chan-

ging between an aperture and the sample, which allowed recording absolute transmission spectra. To identify the relevant features, spectra were normalized by division by the spectrum at the highest magnetic field.

### Syntheses

[$H_2L$]: diisopropylaniline (1.88 mL, 10.0 mmol, 1 eq.) was added to a solution of chloranilic acid (2.09 g, 10.0 mmol, 1 eq.) in acetic acid (30 mL). The resulting mixture was heated to reflux for 2 h. After cooling down to room temperature, water was added to form a purple precipitate which was filtered off and washed with water. The purple residue was dissolved in $CH_2Cl_2$ and dried over $Na_2SO_4$. After removing of the $Na_2SO_4$, the solvent was removed in vacuo to yield the crude product. Recrystallisation from a $CH_2Cl_2$/pentane-mixture (1 : 2) yielded the pure product (1.45 g, 4.18 mmol, 42%). ^{1}H NMR (400 MHz, CDCl$_3$) $\delta$ (ppm):7.92 (s, 1 H, NH), 7.35 (t, $J$ = 7.7 Hz, 1 H, Ar-H), 7.14 (d, $J$ = 7.7 Hz, 2 H, Ar-H), 2.91 (p, $J$ = 6.9 Hz, 2 H, C$\underline{H}$(CH$_3$)$_2$), 1.21 (d, $J$ = 6.9 Hz, 6 H, CH(C$\underline{H}_3$)$_2$), 1.16 (d, $J$ = 6.9 Hz, 6 H, CH(C$\underline{H}_3$)$_2$) (Fig. S7‡). The signal of the OH was not observed. ^{13}C NMR (101 MHz, CDCl$_3$) $\delta$ 175.70, 173.10, 154.47, 146.10, 143.15, 131.55, 129.56, 123.28, 109.64, 101.58, 29.10, 24.19, 22.59 (Fig. S8‡). Th. Anal. Calc. for $C_{18}H_{19}N_1O_3Cl_2$: C 58.71; H 5.20; N 3.80%; found: C 58.84; H 5.24; N 3.92%.

[1]$BF_4$: tmpa (116 mg, 0.40 mmol, 1 eq.) and Fe(BF$_4$)$_2 \cdot 6H_2O$ (135 mg, 0.40 mmol, 1 eq.) were dissolved in MeCN (10 mL) and stirred for 30 min at room temperature. $H_2L$ (148 mg, 0.40 mmol, 1 eq.) and NEt$_3$ (0.5 mL) were added and the resulting mixture was stirred for 2 h at room temperature. The solvent was removed in vacuo. The residue was dissolved in $CH_2Cl_2$ (20 mL) and n-hexane (10 mL) was layered. The resulting green crystals were collected by filtration and dried in vacuo (190 mg, 0.24 mmol, 60%). To yield crystals of [1]$BF_4$ which were suitable for X-ray diffraction, a small sample was dissolved in $CH_2Cl_2$ and slow diffusion of n-pentane into this solution leads to single crystal growth. Th. Anal. Calc. for $C_{36}H_{36}N_5O_3Cl_2BF_4Fe$: C 54.03; H 4.53; N 8.75%; found: C 53.99; H 4.96; N 8.73%.

[2]$BF_4$: tmpa (100 mg, 0.34 mmol, 1 eq.) and Co(BF$_4$)$_2 \cdot 6H_2O$ (117 mg, 0.34 mmol, 1 eq.) were dissolved in MeCN (10 mL) and stirred for 30 min at room temperature. $H_2L$ (128 mg, 0.34 mmol, 1 eq.) and NEt$_3$ (0.3 mL) were added and the resulting mixture was stirred for 2 h at room temperature. The solvent was removed in vacuo. The residue was dissolved in $CH_2Cl_2$ (20 mL) and n-hexane (10 mL) was layered. The resulting red brown crystals were collected by filtration and dried in vacuo (172 mg, 0.22 mmol, 63%). To yield crystals of [2]$BF_4$ which were suitable for X-ray diffraction, a small sample was dissolved in $CH_2Cl_2$ and slow diffusion of n-pentane into this solution leads to single crystal growth. Th. Anal. Calc. for $C_{36}H_{36}N_5O_3Cl_2BF_4Co$: C 53.82; H 4.52; N 8.72%; found: C 53.62; H 4.99; N 8.85%.

[2]$^{2+}$: [2]$^+$ (26 mg, 32 μmol, 1 eq.) was dissolved in MeCN, abs. (5 mL) and NOBF$_4$ (5 mg, 40 μmol, 1.2 eq.) were added. The solution was stirred for 1 h at room temperature resulting

in a color change from brown to green. The solvent was removed *in vacuo* and the residue was dissolved in $CH_2Cl_2$ (6 mL). The resulting solution was filtered and the compound was recrystallized by slow diffusion of *n*-pentane into the resulting solution. The resulting crystalline green material was collected by filtration (15 mg, 15 μmol, 47%).

$^1$H NMR (400 MHz, acetone-d$_6$ (only one isomer)) $\delta$ = 10.92 (s, 1 H, NH), 9.29 (dd, *J* = 6.0, 0.7 Hz, 1 H), 8.55 (dd, *J* = 5.8, 0.7 Hz, 2 H), 8.26 (td, *J* = 7.8, 1.5 Hz, 2 H), 8.06 (td, *J* = 7.7, 1.4 Hz, 1 H), 7.93 (d, *J* = 7.9 Hz, 2 H), 7.88–7.72 (m, 3 H), 7.50 (d, *J* = 0.8 Hz, 1 H), 7.35 (d, *J* = 7.4 Hz, 1 H), 7.17 (d, *J* = 7.8 Hz, 2 H), 5.71 (d, *J* = 16.4 Hz, 2 H, CH$_2$), 5.54 (s, 2 H, CH$_2$), 5.46 (d, *J* = 16.3 Hz, 2 H, CH$_2$), 1.04 (d, *J* = 6.8 Hz, 6 H, CH(CH$_3$)$_2$), 0.94 (d, *J* = 6.8 Hz, 6 H, CH(CH$_3$)$_2$). The signal of the C<u>H</u>(CH$_3$)$_2$ was not detected due to an overlap with the water signal. Anal. Calc. for $C_{36}H_{36}N_5O_3Cl_2B_2F_8Co \cdot 4H_2O \cdot 0.45CH_3CN$: C 45.19; H 4.66; N 7.78%; found: C 45.18; H 4.74; N 7.67%.

## Acknowledgements

## References

1 For selected examples and reviews see: (*a*) M. D. Ward, *Inorg. Chem.*, 1996, **35**, 1712–1714; (*b*) M. Leschke, M. Melter and H. Lang, *Inorg. Chim. Acta*, 2003, **350**, 114–120; (*c*) S. Kitagawa and S. Kawata, *Coord. Chem. Rev.*, 2002, **224**, 11–34; (*d*) J. S. Miller and K. S. Min, *Angew. Chem., Int. Ed.*, 2009, **48**, 262–272; (*e*) B. Therrien, G. Süss-Fink, P. Govindaswamy, A. K. Renfrew and P. J. Dyson, *Angew. Chem., Int. Ed.*, 2008, **47**, 3773–3776; (*f*) K. Heinze, G. Hüttner, L. Zsolnai, A. Jacobi and P. Schober, *Chem. – Eur. J.*, 1997, **3**, 732–743; (*g*) Y.-F. Han, W.-G. Jia, W.-B. Yu and G.-X. Jin, *Chem. Soc. Rev.*, 2009, **38**, 3419–3434; (*h*) Y.-F. Han, H. Li and G.-X. Jin, *Chem. Commun.*, 2010, **46**, 6879.

2 For selected examples see: (*a*) C. Carbonera, A. Dei, J.-F. Létard, C. Sangegrorio and L. Sorace, *Angew. Chem., Int. Ed.*, 2004, **43**, 3136–3138; (*b*) J. Tao, H. Maruyama and O. Sato, *J. Am. Chem. Soc.*, 2006, **128**, 1790–1791; (*c*) B. Li, F.-L. Yang, J. Tao, O. Sato, R.-B. Huang and L.-S. Zheng, *Chem. Commun.*, 2008, 6019–6021.

3 For selected examples see: (*a*) K. S. Min, K. Swierczek, A. G. DiPasquale, A. L. Rheingold, W. M. Reiff, A. M. Atta and J. S. Miller, *Chem. Commun.*, 2008, 317–319; (*b*) K. S. Min, A. G. DiPasquale, A. L. Rheingold and J. S. Miller, *Inorg. Chem.*, 2007, **46**, 1048–1050; (*c*) K. S. Min, A. G. DiPasquale, J. A. Golen, A. L. Rheingold and J. S. Miller, *J. Am. Chem. Soc.*, 2007, **129**, 2360–2368;

4 (*a*) *Spin Crossover in Transition Metal Compounds I-III*, ed. P. Gütlich and H. A. Goodwin, Top. Curr. Chem., Springer, Berlin, Heidelberg, Germany, 2004, vol. 233–235; (*b*) *Eur. J. Inorg. Chem.*, 2013, 574–1067 (cluster issue on spin crossover complexes); (*c*) M. A. Halcrow, *Chem. Soc. Rev.*, 2011, **40**, 4119–4142; (*d*) P. Gütlich, Y. Garcia and H. A. Goodwin, *Chem. Soc. Rev.*, 2000, **29**, 419–427; (*e*) M. Ostermeier, M.-A. Berlin, R. M. Meudtner, S. Demeshko, F. Meyer, C. Limberg and S. Hecht, *Chem. – Eur. J.*, 2010, **16**, 10202–10213.

5 K. S. Min, A. L. Rheingold, A. G. DiPasquale and J. S. Miller, *Inorg. Chem.*, 2006, **45**, 6135–6137.

6 (*a*) D. Schweinfurth, H. S. Das, F. Weisser, D. Bubrin and B. Sarkar, *Inorg. Chem.*, 2011, **50**, 1150–1159; (*b*) F. Weisser, R. Hübner, D. Schweinfurth and B. Sarkar, *Chem. – Eur. J.*, 2011, **17**, 5727–5736; (*c*) D. Schweinfurth, M. M. Khusniyarov, D. Bubrin, S. Hohloch, C.-Y. Su and B. Sarkar, *Inorg. Chem.*, 2013, **52**, 10332–10339; (*d*) D. Schweinfurth, Y. Rechkemmer, S. Hohloch, N. Deibel, I. Peremykin, J. Fiedler, R. Marx, P. Neugebauer, J. van Slageren and B. Sarkar, *Chem. – Eur. J.*, 2014, **20**, 3475–3486; (*e*) M. G. Sommer, D. Schweinfurth, F. Weisser, S. Hohloch and B. Sarkar, *Organometallics*, 2013, **32**, 2069–2078; (*f*) N. Deibel, M. G. Sommer, S. Hohloch, J. Schwann, D. Schweinfurth, F. Ehret and B. Sarkar, *Organometallics*, 2014, **33**, 4756–4765; (*g*) N. Deibel, S. Hohloch, D. Schweinfurth, F. Weisser, A. Grupp and B. Sarkar, *Chem. – Eur. J.*, 2014, **20**, 15178–15187; (*h*) B. Sarkar, D. Schweinfurth, N. Deibel and F. Weisser, *Coord. Chem. Rev.*, 2015, **293–294**, 250–262; (*i*) D. Schweinfurth, F. Weisser and B. Sarkar, *Nachr. Chem.*, 2009, **57**, 862–866; (*j*) H. S. Das, F. Weisser, D. Schweinfurth, C.-Y. Su, L. Bogani, J. Fiedler and B. Sarkar, *Chem. – Eur. J.*, 2010, **16**, 2977–2981; (*k*) H. S. Das, D. Schweinfurth, J. Fiedler, M. M. Khusniyarov, S. M. Mobin and B. Sarkar, *Chem. – Eur. J.*, 2014, **20**, 4334–4346; (*l*) D. Gupta, V. Singh, S. Hohloch, M. Sathiyendiran, K. Tedin and B. Sarkar, *Polyhedron*, 2015, **100**, 243–250.

7 (*a*) H. S. Das, A. K. Das, R. Pattacini, R. Huebner, B. Sarkar and P. Braunstein, *Chem. Commun.*, 2009, 4387–4389; (*b*) P. Braunstein, D. Bubrin and B. Sarkar, *Inorg. Chem.*, 2009, **48**, 2534–2540; (*c*) A. Paretzki, R. Pattacini, R. Huebner, P. Braunstein and B. Sarkar, *Chem. Commun.*, 2010, **46**, 1497–1499; (*d*) N. Deibel, D. Schweinfurth, R. Huebner, P. Braunstein and B. Sarkar, *Dalton Trans.*, 2011, **40**, 431–436; (*e*) S. Hohloch, P. Braunstein and B. Sarkar, *Eur. J. Inorg. Chem.*, 2012, 546–553; (*f*) N. Deibel, S. Hohloch, M. G. Sommer, D. Schweinfurth, F. Ehret, P. Braunstein and B. Sarkar, *Organometallics*, 2013, **32**, 7366–7375; (*g*) F. Yuan, F. Weisser, B. Sarkar, A. Garci, P. Braunstein, L. Routaboul and B. Therrien, *Organometallics*, 2014, **33**, 5043–5045.

8 (*a*) K. Heinze, G. Huttner and L. Zsolnai, *Z. Naturforsch.*, 1999, 1147–1154; (*b*) D. Kumbhakar, B. Sarkar, S. Maji,

S. M. Mobin, J. Fiedler, F. A. Urbanos, R. Jimenez-Aparicio, W. Kaim and G. K. Lahiri, *J. Am. Chem. Soc.*, 2008, **130**, 17575–17583; (*c*) T. E. Keyes, R. J. Forster, P. W. Jayaweera, C. G. Coates, J. J. McGarvey and J. G. Vos, *Inorg. Chem.*, 1998, **37**, 5925–5932; (*d*) G. Margraf, T. Kretz, F. F. de Biani, F. Lashi, S. Losi, P. Zanello, J. W. Bats, B. Wolf, K. Removic-Langer, M. Lang, A. Prokofiev, W. Assmus, H.-W. Lerner and M. Wagner, *Inorg. Chem.*, 2006, **45**, 1277–1288; (*e*) S. Scheuermann, B. Sarkar, M. Bolte, J.-W. Bats, H.-W. Lerner and M. Wagner, *Inorg. Chem.*, 2009, **48**, 9385–9392; (*f*) P. Braunstein, O. Siri, J.-P. Taquet, M.-M. Rohmer, M. Bénard and R. J. Walter, *J. Am. Chem. Soc.*, 2003, **125**, 12246–12256; (*g*) Q.-Z. Yang, O. Siri and P. Braunstein, *Chem. Commun.*, 2005, 2660–2662; (*h*) Q.-Z. Yang, O. Siri and P. Braunstein, *Chem. – Eur. J.*, 2005, **11**, 7237–7246; (*i*) O. Siri, J.-P. Taquet, J.-P. Collin, M.-M. Rohmer, M. Bénard and P. Braunstein, *Chem. – Eur. J.*, 2005, **11**, 7247–7253; (*j*) F. A. Cotton, J.-Y. Jin, Z. Li, C. A. Murillo and J. H. Reibenspies, *Chem. Commun.*, 2008, 211–213; (*k*) S. Kar, B. Sarkar, S. Ghumaan, D. Janardanan, J. van Slageren, J. Fiedler, V. G. Puranik, R. B. Sunoj, W. Kaim and G. K. Lahiri, *Chem. – Eur. J.*, 2005, **11**, 4901–4911.

9 G. Aromi, D. Aguila, P. Gamez, F. Luis and O. Roubeau, *Chem. Soc. Rev.*, 2012, **41**, 537–546.

10 (*a*) I. Salitros, O. Fuhr, R. Kruk, J. Pavlik, L. Pogany, B. Schäfer, M. Tatarco, R. Boca, W. Linert and M. Ruben, *Eur. J. Inorg. Chem.*, 2013, 1049–1057; (*b*) F. Varret, S. A. Salunke, K. Boukheddaden, A. Boussekksau, E. Codjovi, C. Enachescu and J. Linares, *C. R. Chim.*, 2003, 385–393.

11 S. Decartins, P. Gütlich, C. P. Köhler, H. Spieringand and A. Hauser, *Chem. Phys. Lett.*, 1984, **105**, 1–4.

12 (*a*) V. Ksenofontov, A. B. Gaspar and P. Gütlich, *Top. Curr. Chem.*, 2004, **235**, 23–64; (*b*) J. A. Real, A. B. Gaspar, A. Niel and M. C. Munoz, *Coord. Chem. Rev.*, 2003, **1–2**, 121–141; (*c*) A. Bencini, A. Caneschi, C. Carbonera, A. Dei, D. Gatteschi, R. Righini, C. Sangregorio and J. van Slageren, *J. Mol. Struct.*, 2003, **656**, 141–154; (*d*) A. Caneschi, A. Dei, F. F. de Biani, P. Gütlich, V. Ksenofontov, G. Levshenko, A. Hoefer and F. Renz, *Chem. – Eur. J.*, 2001, **7**, 3926–3930.

13 (*a*) A. Bencini, A. Beni, F. Costantino, A. Dei, D. Gatteschi and L. Sorace, *Dalton Trans.*, 2006, 722–729; (*b*) Y. Mulyana, G. Poneti, B. Moubaraki, K. S. Murray, B. F. Abrahams, L. Sorace and C. Boscovic, *Dalton Trans.*, 2010, **39**, 4757–4767.

14 (*a*) D. N. Hendrickson and C. G. Pierpont, *Top. Curr. Chem.*, 2004, **234**, 63–95; (*b*) D. Schweinfurth, F. Weisser, D. Bubrin, L. Bogani and B. Sarkar, *Inorg. Chem.*, 2011, **50**, 6114–6121.

15 M. D. Ward and J. A. McCleverty, *J. Chem. Soc., Dalton Trans.*, 2002, 275–288.

16 A. L. Ward, L. Elbaz, J. B. Kerr and J. Arnold, *Inorg. Chem.*, 2012, **51**, 4694–4706.

17 M. Krejcik, M. Danek and F. Hartl, *J. Electroanal. Chem.*, 1991, **317**, 179–187.

18 (*a*) G. M. Sheldrick, *Acta Crystallogr., Sect. C: Cryst. Struct. Commun.*, 2015, **71**, 3–8; (*b*) *X-RED*, STOE & CIE GmbH, Darmstadt, Germany, 2002; (*c*) G. M. Sheldrick, *SADABS Ver., 2008/1; SADABS. Program for Empirical Absorption Correction*, University of Gottingen, Germany.

19 (*a*) E. M. Schubert, *J. Chem. Educ.*, 1992, **69**, 62; (*b*) D. F. Evans, *J. Chem. Soc.*, 1959, 2003–2005; (*c*) G. A. Bain and J. F. Berry, *J. Chem. Educ.*, 2008, **85**, 532–536.

20 S. Stoll and A. Schweiger, *J. Magn. Reson.*, 2006, **178**, 42–55.